This article is made available via the ACS COVID-19 subset for unrestricted RESEARCH re-use and analyses in any form or by any means with acknowledgement of the original source. These permissions are granted for the duration of the World Health Organization (WHO) declaration of COVID-19 as a global pandemic.

JCIM JOURNAL OF CHEMICAL INFORMATION AND MODELING

pubs.acs.org/jcim Article

Effect of an Inhibitor on the ACE2-Receptor-Binding Domain of SARS-CoV-2

Gaurav Sharma, Lin Frank Song, and Kenneth M. Merz*

Cite This: https://doi.org/10.1021/acs.jcim.1c01283 Read Online

ACCESS | Metrics & More | Article Recommendations | Supporting Information

ABSTRACT: The recent outbreak of COVID-19 infection started in Wuhan, China, and spread across China and beyond. Since the WHO declared COVID-19 a pandemic (March 11, 2020), three vaccines and only one antiviral drug (remdesivir) have been approved (Oct 22, 2020) by the FDA. The coronavirus enters human epithelial cells by the binding of the densely glycosylated fusion spike protein (S protein) to a receptor (angiotensin-converting enzyme 2, ACE2) on the host cell surface. Therefore, inhibiting the viral entry is a promising treatment pathway for preventing or ameliorating the effects of COVID-19 infection. In the current work, we have used all-atom molecular dynamics (MD) simulations to investigate the influence of the MLN-4760 inhibitor on the conformational properties of ACE2 and its interaction with the receptor-binding domain (RBD) of SARS-CoV-2. We have found that the presence of an inhibitor tends to completely/partially open the ACE2 receptor where the two subdomains (I and II) move away from each other, while the absence results in partial or complete closure. The current study increases our understanding of ACE inhibition by MLN-4760 and how it modulates the conformational properties of ACE2.

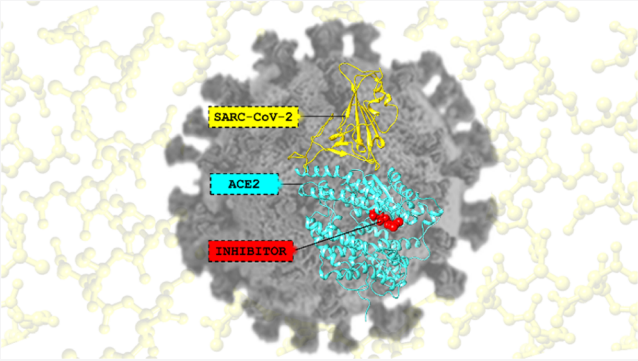

1. INTRODUCTION

In December 2019, a novel coronavirus appeared in China and caused an acute respiratory disease now called coronavirus disease 2019 (COVID-19). The virus is a betacoronavirus associated with severe acute respiratory syndrome coronavirus (SARS-CoV), which has led to the name SARS-CoV-2.[1] In the last 20 years, the virus is the third known coronavirus that crosses the species barrier and causes highly pathogenic and deadly diseases, namely, severe respiratory infection in humans (SARS-CoV) and the Middle East respiratory syndrome coronavirus (MERS-CoV) in 2003 and 2012, respectively.[2,3] Due to the quick increase in the number of cases globally, the World Health Organization has declared it a pandemic.[4]

The SARS-CoV-2 enters human epithelial cells through the binding of the densely glycosylated fusion spike protein (S protein) to a receptor (angiotensin-converting enzyme 2, ACE2) on the host cell surface.[5] ACE2 is a zinc-containing metalloenzyme belonging to the renin−angiotensin system (RAS) and lowers blood pressure by catalyzing the hydrolysis of angiotensin II into angiotensin (1−7).[6] The extracellular region of the ACE2 enzyme contains two domains, i.e., a zinc-containing peptidase domain (PD, residues 19−611) and a collectrin domain (CLD, residues 612−740) shown in Figure 1A.[5,6] The PD is further divided into two subdomains (I and II) (Figure 1B), which form the two sides of a clamshell-like structure with a deep cleft in the center.[6] The two subdomains contain the active site and undergo a large substrate-dependent hinge-bending movement to catalyze the hydrolysis of angiotensin II into angiotensin (1−7).[6] This movement of ACE2 exists in two orientations: a substrate/inhibitor-bound ("closed") and unbound ("open") conformation.[6] Site-directed mutagenesis study[7] highlighted that the active site is composed of a Zn^{2+} ion coordinated to H374, H378, E402, and water molecules, as shown in Figure 1C. In addition, two 2nd coordination shell residues (H345 and H505) aid in the stabilization of the enzyme−substrate complex by forming a network of hydrogen-bond interactions.[7] According to the proposed catalytic mechanism, the substrate binds to the Zn^{2+} ion and forms an enzyme−substrate complex by forming a tetrahedral intermediate.[6] This causes a ∼16° subdomain hinge-bending movement of subdomain I toward subdomain II.[6] Simultaneously, H505 transfers a proton to the nitrogen atom of the scissile peptide resulting in its cleavage.[6]

The binding of the S protein S1 subunit to ACE2 is triggered by the destabilization of the prefusion trimer, inducing the shedding of the S1 and transition of the S2 subunit to a highly

Special Issue: Advancing Women in Chemistry

Received: October 22, 2021

 © XXXX American Chemical Society

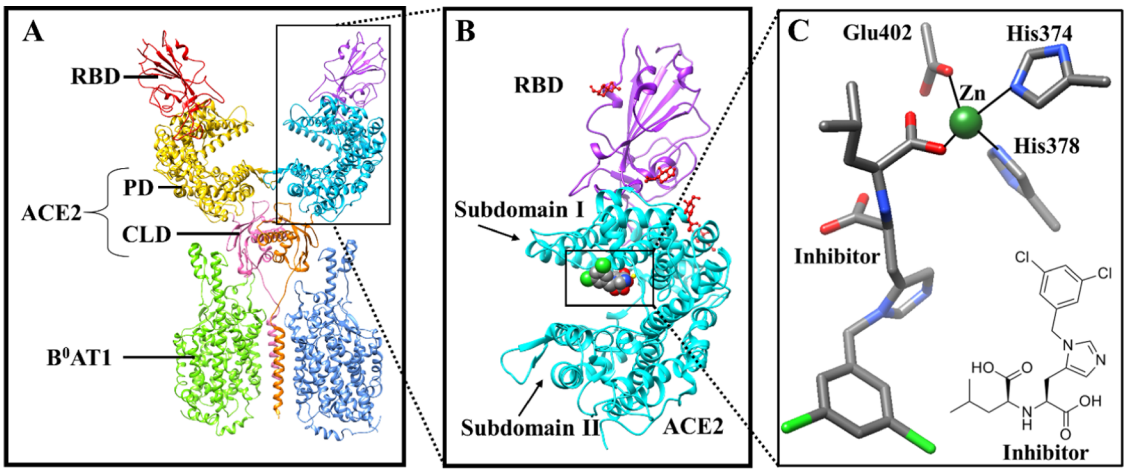

Figure 1. (A) X-ray structure of the RBD−ACE2−B^0AT1 complex. RBD: Receptor-binding domain, PD: peptidase domain, and CLD: collectrin-like domain. (B) Inhibitor-bound ACE2−RBD complex ($\mathbf{RA}'_O$). (C) Inhibitor bound to the monomeric ACE2 active site.

stable post-fusion conformation.[8,9] To engage the ACE2 receptor, the receptor-binding domain (RBD) of the S1 subunit does a hinge-like movement transiently exposing the receptor-binding site.[6] The hinge-like movement is referred to as "down" and "up" conformations, where "down" corresponds to the receptor-inaccessible state and "up" corresponds to the receptor-accessible state, which is thought to be less stable.[5] The RBD contains two parts: (1) a twisted five-stranded antiparallel β sheet (β1, β2, β3, β4, and β7) forming the core and (2) a receptor-binding membrane (RBM, β5, and β6) that binds to the ACE2 surface (Figure S1).[5] At the ACE2−RBD interface, a total of 17 residues of the RBM connect to the 20 residues of ACE2.[5] Comparative analysis on the SARS-CoV and SARS-CoV-2 interaction with the ACE2 enzyme suggested a higher binding affinity of SARS-CoV-2 toward ACE2,[10−13] while two separate studies proposed that both have a similar binding affinity.[14,15] Any modification in the ACE2 structure should affect this interface and hence the ACE2−RBD binding, presenting an avenue to create therapeutic agents against SARS-CoV-2.

Currently, more than 350 clinical trials are underway out of which remdesivir and Nirmatrelvir are is the only drug recently approved by the FDA for COVID-19 treatment.[16] The present pharmacotherapy adopted by the FDA is divided into three categories: (1) antiviral therapy, e.g., remdesivir;[16,17] (2) immune-based therapy such as human blood-derived products and plasma;[18−20] and (3) immunomodulators like corticosteroids.[16,21] Antiviral therapy is more effective when applied early in the course of illness before it progresses into the hyperinflammatory state, while the immune-based and immunomodulating therapy is encouraging in the later stages of the disease.[17] Therefore, antiviral therapy is more auspicious in combating the disease in comparison to other treatment strategies. It works by restricting the viral replication by inhibiting the entry and the activity of 3-chymotrypsin-like protease ($3CL^{pro}$) and the papain-like cysteine protease (PL^{pro}) enzymes present in the coronavirus.[16,22−25] The first step of the viral life cycle is its entry into the cell.[26] Consequently, blocking the viral entry can successfully prevent/delay the destruction of the immune system and reduce the severity and at least delay disease progression/death if not fully halting the progression of the infection.[26] A relevant example is an antiretroviral drug maraviroc, which binds to the human cell membrane receptor preventing the virus−receptor interaction and thereby inhibits the virus entry into the cell.[27] Three major approaches have recently been explored to inhibit the coronavirus endocytosis. The first approach is making antibodies that can effectively bind to the S-proteins.[15,28−30] Second is inhibiting the ACE2−RBD interaction by binding a compound at the interface. The third and less investigated approach is the development of inhibitors that modify the secondary structure of ACE2.

In the COVID-19 drug discovery process, special emphasis is given to drug repurposing (i.e., older drugs, new uses).[31−39] As the drugs are already in the market time can be saved by avoiding expensive pharmacokinetic, pharmacodynamic, and toxicity studies.[40,41] High-throughput virtual screening (HTVS), molecular docking, and molecular dynamics (MD) simulations have been widely used to explore FDA-approved drugs against the S-proteins, ACE2−RBD interface, and main protease. For instance, Choudhary et. al have used HTVS, molecular docking, and MD simulations to investigate the FDA-approved LOPAC drug library against RBD and the ACE2 receptor.[42] Likewise, Maffucci et al. utilized similar techniques on 3000 existing drugs targeting the main protease and S-proteins.[43] Moreover, FDA-approved drugs,[44] alkamides and piperamides,[45] amino acids,[46] peptides,[47,48] and various natural products[49−52] have been suggested as potential inhibitors of the coronavirus. In addition, kobophenol A found to block the interaction between ACE2 and RBD with an IC_{50} of 1.81 μM.[51] Till now, there are ten vaccines approved by WHO. For instance, Pfizer−BioNTech and Moderna COVID-19 vaccines are composed of nucleoside-modified mRNA encoding a mutated form of the S protein.[53,54] They have shown 95 and 94% efficacy against the disease, respectively.[54,55] On the other hand, Oxford−AstraZeneca vaccine is a viral vector vaccine with a lower efficacy of 85%.[56,57] Others include are Janssen Vaccines (nonreplicating viral vector),[58] CoronaVac (inactivated vaccine),[59] BBIBP-CorV (inactivated vaccine),[60] and Covidshield (viral vector).[61]

Due to the late discovery of the ACE2 enzyme in the year 2000[62,63] (ACE in 1956[64]), there are no clinically approved ACE2 inhibiting drugs. In 2002, Dales et al. developed the first potent and selective picomolar ACE2 inhibitor (MLN-4760)[65] causing its hinge-bending inhibition.[6] Subsequently, various other ACE2 inhibitors have been proposed experimentally[66−69] and computationally.[51,70−76] As ACE2 is a component of the renin−angiotensin−aldosterone system (RAAS), the primary

https://doi.org/10.1021/acs.jcim.1c01283
J. Chem. Inf. Model. XXXX, XXX, XXX−XXX

goal of these studies was to regulate blood pressure by modulating the angiotensin II levels in the kidney. However, none of them has so far reached clinical trials despite years of research to date. Before the progression of COVID-19, very few computational studies of ACE2 inhibitors have been performed. Huentelman et al. in 2004 utilized the molecular docking approach to identify the ACE2 inhibitor (*N*-(2-aminoethyl)-1 aziridine-ethanamine).[71] A different group in 2012 employed a similar protocol to design seven ACE2 inhibitors.[77] Recently, a short simulation (100 ns) of the MLN-4760 inhibitor effect on the interaction of RBD and ACE2 has been performed by Nami et al., which showed that it neither blocked nor increased the binding of the SARS-CoV-2 spike RBD to human ACE2 and probably had no effect on the viral entry.[78] Cao et al. have designed sequences of few amino acids that can inhibit the interactions between ACE2 and RBD.[79] Similarly, Mehranfar et al. designed a sequence of a few amino acids and functionalized with gold nanoparticles as antivirals to prevent the viral entry.[80] Raghavan et al. suggested that metadichol can inhibit the ACE2 enzyme.[81] Molecular dynamics studies and binding enthalpy calculations suggest that the binding enthalpy could be reduced for the S protein−ACE2 interface in the presence of the MLN-4760 inhibitor.[82] This weakening of binding strength was proposed as a result of the destabilization of the interactions between ACE2 and RBD.[82] A comparison of ACE2−RBD interactions in the SARS-CoV-1 and SARS-CoV-2 complexes performed by MD simulations shows that the latter has stronger interface interactions.[83] Understanding the effect of inhibitors on ACE2 is of key importance in elucidating the ACE2−RBD interaction and in designing new functional inhibitors.

Despite a considerable amount of computational and experimental data, the precise molecular details of the ACE2−RBD interactions and the effect of the inhibitor on ACE2 remain open. To explore these knowledge gaps, we have utilized all-atom molecular dynamics (MD) simulations to study the influence of the MLN-4760 inhibitor on the conformational properties of ACE2 and its interaction with the RBD of SARS-CoV-2. Moreover, different conformations (open and closed) of the ACE2 enzyme have also been explored. With these insights, we present a model of how an ACE2 inhibitor can affect its structure and hence its interaction with the spike protein and ultimately blocking the virus entry. The current analysis will increase our understanding of ACE inhibition by MLN-4760 and will explore how these inhibitors alter the nature of the ACE2/SARS-CoV-2 interface and if exploiting conformational changes at this interface might affect SARS-CoV-2 infectivity. In what follows we first discuss the computational protocol, followed by a detailed analysis of the effect of the inhibitor on the ACE2 and ACE2−RBD interface. Finally, the opening and closing mechanisms of the ACE2 enzyme have been proposed.

2. COMPUTATIONAL DETAILS

2.1. Modeling. The crystal structure of the SARS-CoV-2 spike protein receptor-binding domain (RBD) bound to the ACE2 receptor was obtained from the protein data bank (PDB ID: 6M0J).[5] In this ACE2−RBD structure, four additional *N*-acetyl-*β*-glucosaminide (NAG) glycans linked to ACE2 N90, N322, and N546 and RBD N343 were also present. These glycans are suggested to control the conformational plasticity of the RBD.[84−86] In addition, the effect of *N*-glycan size was also analyzed by placing glycans of larger size (Figure S2). Although it is proposed that the *N*-glycans play an important structural role in modulating the conformational dynamics of RBD and regulating the ACE2 recognition,[84] it does not seem to affect the ACE2−RBD complex once the interaction is formed. The superposition of the $\mathbf{RA_O}$ and $\mathbf{RA'_O}$ models to their respective larger *N*-glycan structures does not show a major structural difference (Figure S3). To this complex, the MLN-4760 inhibitor (taken from an inhibitor-bound ACE2 structure; PDB ID: 1R4L[6]) was married into the binding site by aligning the active site residues using the VMD program package.[87] The hydrogen atoms of the inhibitor were added using the protein preparation wizard from the Schrodinger suite 2019-4,[88] resulting in a total net charge of −1. The AM1-BCC charges were calculated using the Antechamber in the AmberTools19,[89] and then the GAFF 2.11[90] was used to describe the atom types and generate the bonded and nonbonded parameters. The H++ server[91] was used to determine the protonation states of the amino acids and a careful examination of charged groups was carried out. The ff14SB[92] and GLYCAM 06j-1[93] force fields were employed in the construction of the topology files for the protein and glycans, respectively. The system was solvated using the TIP3P water,[94] with a minimum distance of 10 Å between the edge of the cell and solute atoms. Charge neutrality was maintained by adding an appropriate number of Na^+ ions. The Zn^{2+} ion in the active site, the crystalized Cl^- ion, and the neutralizing Na^+ ions were described by IOD parameter sets[95,96] developed previously in our group. Besides the ACE2−RBD complex, simulations of only the ACE2 receptor (open and closed conformations) were also performed. The closed conformation inhibitor-bound ACE2 structure was obtained from the protein data bank (PDB ID: 1R4L[6]). The disordered segment of collectrin homology domains present in this structure was deleted using the VMD software.[87] On the other hand, the open conformation inhibitor-bound ACE2 structure was obtained by removing the RBD from the ACE2−RBD complex. To compare the effect of the inhibitor on the ACE2 receptor, simulations of the apo form (without the inhibitor) of the above three complexes were also performed. Overall, we have simulated six different complexes, and for the ease of simplicity, the complexes are labeled as (a) $\mathbf{A_O}$: open conformation of ACE2; (b) $\mathbf{A_C}$: closed conformation of ACE2; and (c) $\mathbf{RA_O}$: RBD bound open conformation of ACE2 and their respective inhibitor-bound structures ($\mathbf{A'_O}$, $\mathbf{A'_C}$, $\mathbf{RA'_O}$). Moreover, the $\mathbf{A'_C}$ complex exists in two different states, i.e., closed for the first 500 ns and open for the last 500 ns. Therefore, in this paper, the closed state of $\mathbf{A'_C}$ is labeled as $\mathbf{A'_{C1}}$ and the open state is labeled as $\mathbf{A'_{C2}}$.

2.2. Molecular Dynamics Simulations. The molecular dynamics (MD) simulations were performed using the AMBER18[89] program package. For each simulation, five steps of minimization were first performed to remove close contacts. The first step minimizes the water molecules and counterions, with the protein restrained. In the second, third, and fourth steps, the heavy atoms, backbone heavy atoms, and backbone carbon and oxygen atoms of the protein were restrained, while the last step minimizes the entire system. Each minimization step consisted of 10 000 cycles of steepest descent and 10 000 cycles of conjugate gradient minimization. Afterward, the system was heated from 0 to 300 K gradually for 1 ns under constant NVT conditions. The solute was restrained using a 5 kcal/(mol·Å^2) restraining potential. Finally, the system was equilibrated at 300 K for 6 ns employing the NPT ensemble, with the restraining potential gradually released. Finally, 1 μs of sampling at 300 K under constant NPT conditions was performed. The Langevin thermostat with a collision frequency of 2 ps^{-1} was

https://doi.org/10.1021/acs.jcim.1c01283
J. Chem. Inf. Model. XXXX, XXX, XXX−XXX

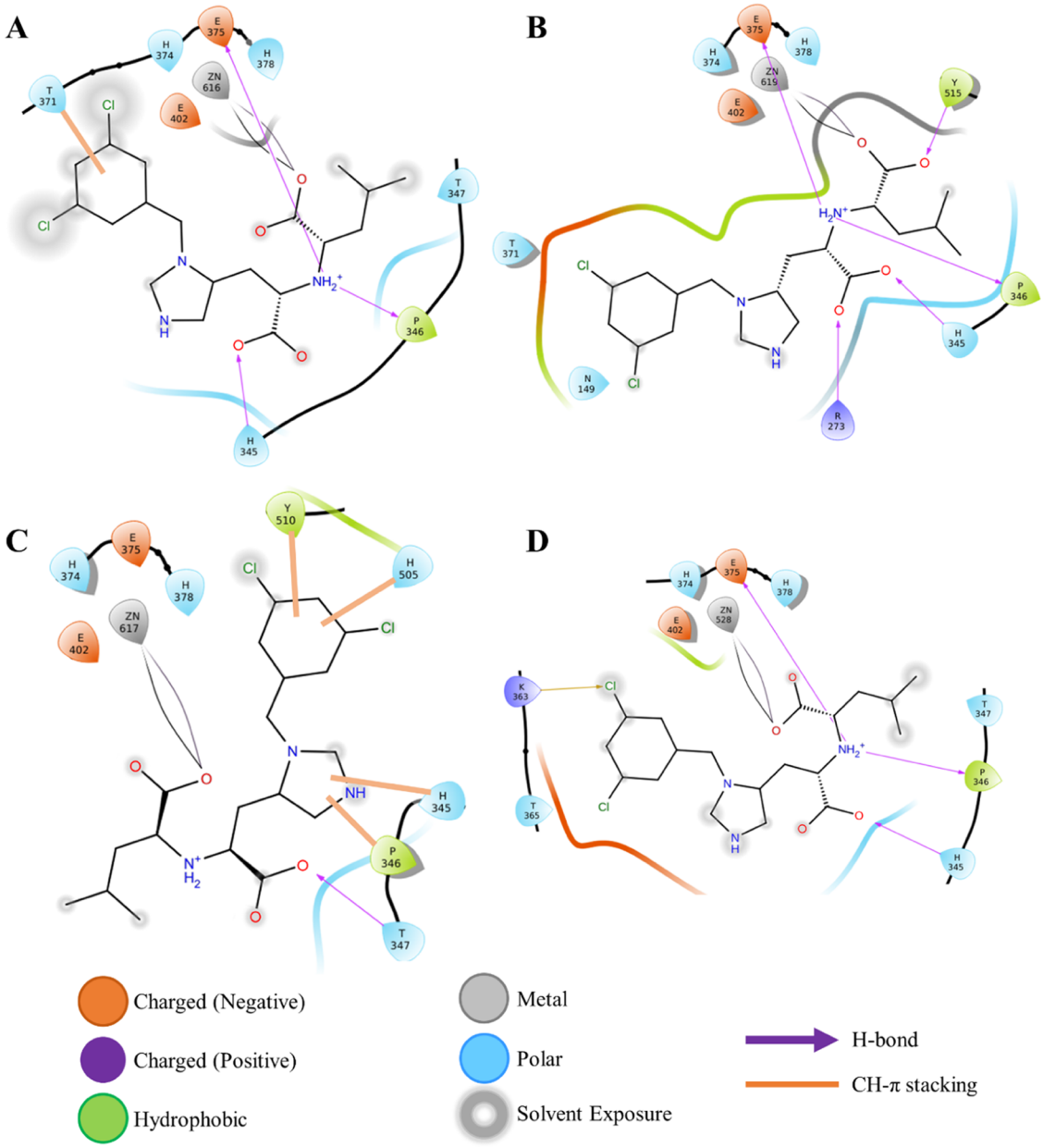

Figure 2. ACE2−inhibitor 2D interaction graph. (A) ACE2 open complex ($\mathbf{A}'_{\mathrm{O}}$); (B) ACE2 closed complex ($\mathbf{A}'_{\mathrm{C1}}$); (C) ACE2 open complex ($\mathbf{A}'_{\mathrm{C2}}$); and (D) ACE2−RBD complex ($\mathbf{RA}'_{\mathrm{O}}$).

used to control the temperature, and the Berendsen barostat with a pressure relaxation time of 5 ps was used for the pressure control. The time step was 2 fs and the nonbonded cutoff of 10 Å. The SHAKE[97] algorithm was used to constrain bonds involving hydrogen atoms. We conducted two simulations each for all systems.

2.3. Simulation Analysis. The electrostatic surface potential (ESP) of the inhibitor was computed at the B3LYP[98]/6-31G(d)[99] level using the Gaussian 16 program.[100] Cluster analysis was utilized to obtain the most representative structures from the MD simulations. The hydrophobicity surface potential of the complexes was obtained using the UCSF Chimera program.[101] Porcupine plots obtained from the PyMOL program[102] were utilized to explore modes of protein motion. The Maestro software[103] was used to create the two-dimensional (2D) interaction diagram between the enzyme and the inhibitor. To examine the secondary structure of the protein, we used the Define Secondary Structure of Proteins (DSSP) algorithm. The helical wheel projection of α2 and α3 helices of the ACE2 receptor was obtained from the NetWheel online web server.[104] The VMD,[87] Schrodinger suite 2019-4,[88] and UCSF Chimera[101] programs were used for the visualization of the MD trajectories and preparation of the figures used in this study.

3. RESULTS AND DISCUSSION

We have used 1 μs long all-atom MD simulations to investigate the interaction of the peptidase domain (PD) of the ACE2 enzyme with the receptor-binding domain (RBD) of the SARS-CoV-2 spike protein. Experimental studies have suggested that the RBD interacts strongly with the ACE2. These strong interactions are mediated mainly through electrostatic complementarity (indicated by the hydrophobicity surface (Figure S4)), hydrogen bonding, and hydrophilic interactions. Finally, to compare these results, different conformations of ACE2 (i.e.,

https://doi.org/10.1021/acs.jcim.1c01283
J. Chem. Inf. Model. XXXX, XXX, XXX−XXX

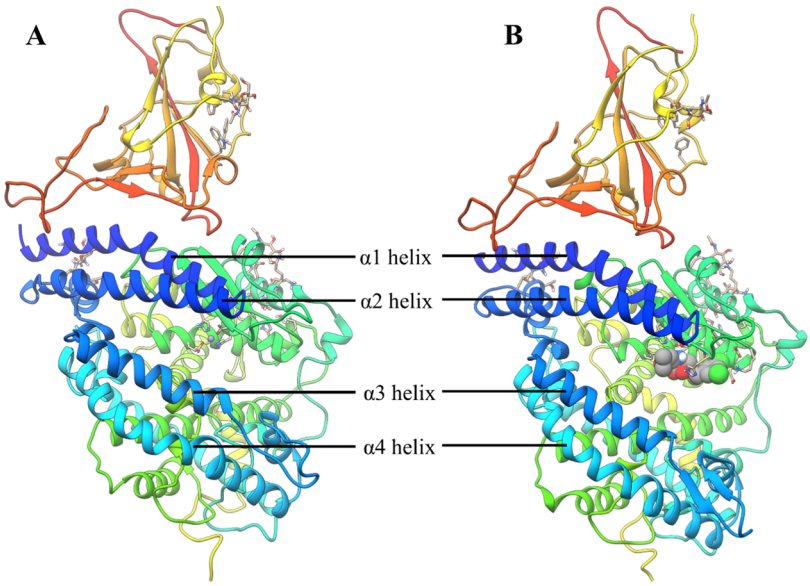

Figure 3. Equilibrated structure of (A) ACE2−RBD ($\mathbf{RA_O}$) and (B) ACE2−RBD−inhibitor ($\mathbf{RA'_O}$) complex.

open and closed states) were also elucidated. The analysis of the root-mean-square deviations (RMSDs) confirmed the equilibration of all of the complexes (i.e., $\mathbf{A_O}$, $\mathbf{A_C}$, $\mathbf{RA_O}$) and their respective inhibitor-bound structures (i.e., $\mathbf{A'_O}$, $\mathbf{A'_C}$, $\mathbf{RA'_O}$) within the simulation time (Figure S5). The interactions and structural changes in the ACE2 enzyme and RBD have been discussed by comparing the secondary structures, noncovalent interactions, hydrogen bonding, root-mean-square fluctuations (RMSFs), and helical wheel projection.

3.1. Binding Mode of the Inhibitor. Continuing the analysis of the MD trajectories, we evaluated the specific interactions between the MLN-4760 inhibitor and the ACE2 receptor. MLN-4760 is a negatively charged His−Leu mimetic inhibitor with an imidazole ring, an isobutyl side chain, two carboxylate groups, and a dichlorobenzyl group (Figures 1C and S6).[65] The imidazole ring mimics His, isobutyl as the Leu side chain, Leu carboxylate group binds to the Zn^{2+} ion, while His carboxylate group mimics the zinc-bound tetrahedral intermediate formed during the peptide hydrolysis. The inhibitor binds to the active site located on the subdomain I of ACE2. Gangadevi et al. have shown that a natural compound Kobophenol A is an inhibitor with an IC_{50} of 1.81 μM, which they suggest bind in the hydrophobic cavity (between the two clamshells) of ACE2.[51] In the $\mathbf{RA'_O}$ complex, on inhibitor binding, the 3,5-dichlorobenzyl and isobutyl side chains get exposed to the solvent, while the two carboxyl groups were buried inside the binding cleft to interact with the active site (Figure 2D); this is because the open conformation of ACE2 allows water molecules to access the active site, as shown in Figure S7. Likewise, in other ACE2 open conformations [$\mathbf{A'_O}$ and $\mathbf{A'_{C2}}$], the 3,5-dichlorobenzyl and isobutyl side chains were solvent-exposed, and the carboxyl groups were buried (Figure 2A−D). To accommodate the inhibitor, the active site residues fluctuate, and the magnitude depends on the change in the ACE2 conformational state (i.e., changing from the closed to open form). For instance, in the $\mathbf{RA'_O}$ (partial ACE2 opening) and $\mathbf{A'_{C2}}$ (complete opening of ACE2) complexes, major fluctuations were observed in the active site residues (Figures 2 and S8). This is not surprising since in these structures the ACE2 is changing from one state to another. On the other hand, in $\mathbf{A'_O}$ and $\mathbf{A'_{C1}}$ complexes, almost no fluctuations were identified in the active site residues (Figure S8). Close inspection of the $\mathbf{RA'_O}$ 2D graph (Figure 2D) of the residues located within 6 Å of the negatively charged inhibitor highlighted that the binding is likely to be driven by its interaction with the Zn^{2+} ion, H345, P346, T347, K363, T365, and E375, indicating their active role in binding. These residues form four hydrogen bonds with the inhibitor. Importantly, residue H345, suggested as a hydrogen-bond donor/acceptor in the formation of the tetrahedral peptide intermediate,[7,67] forms a hydrogen-bond (1.8 Å) interaction with the carboxyl group of the inhibitor. However, residue H505 proposed to stabilize the reactant during catalysis[7] was at ∼6.1 Å from the inhibitor (Figure S9). This is because $\mathbf{RA'_O}$ is in the open state making the H505 move far from the vicinity of the inhibitor. In the $\mathbf{A'_O}$ complex, three hydrogen bonds were found, while five bonds were detected in $\mathbf{A'_{C1}}$ and only one in $\mathbf{A'_{C2}}$. Again, this difference is due to the change of the ACE2 state (from closed to open) due to inhibitor binding. Interestingly, in the $\mathbf{A'_C}$ complex, the inhibitor binding causes a conformational change in the structure of the ACE2 protein that eventually leads to the opening of the two subdomains and subsequent water flux into the active site. In this structure, for the first 500 ns, the inhibitor was planar and ACE2 was in a closed conformation, while for the rest of the 500 ns, the inhibitor undergoes an angle rotation promoting the opening of the ACE2 flaps (Figure S10). The angle rotation in the inhibitor results in the loss of four H-bonds and the formation of four CH−π interactions between the active site and inhibitor.

Overall, the binding of the inhibitor results in the reorganization of the active site and the movement of the α-helix (α1−α4) chains promoting the complete/partial opening of the ACE2 receptor.

3.2. Fluctuations in ACE2 Due to Inhibitor Binding. In the open conformation of the ACE2, the upper and the lower subdomains are ∼13 Å apart, while in the closed conformation, the two subdomains come close to each other.[6] The most representative structure of the $\mathbf{RA'_O}$ complex obtained from the last 800 ns simulation is shown in Figure 3B. In all of the simulations, fluctuations were observed in the subdomains I and II of the ACE2 receptor. These fluctuations were also detected

https://doi.org/10.1021/acs.jcim.1c01283
J. Chem. Inf. Model. XXXX, XXX, XXX−XXX

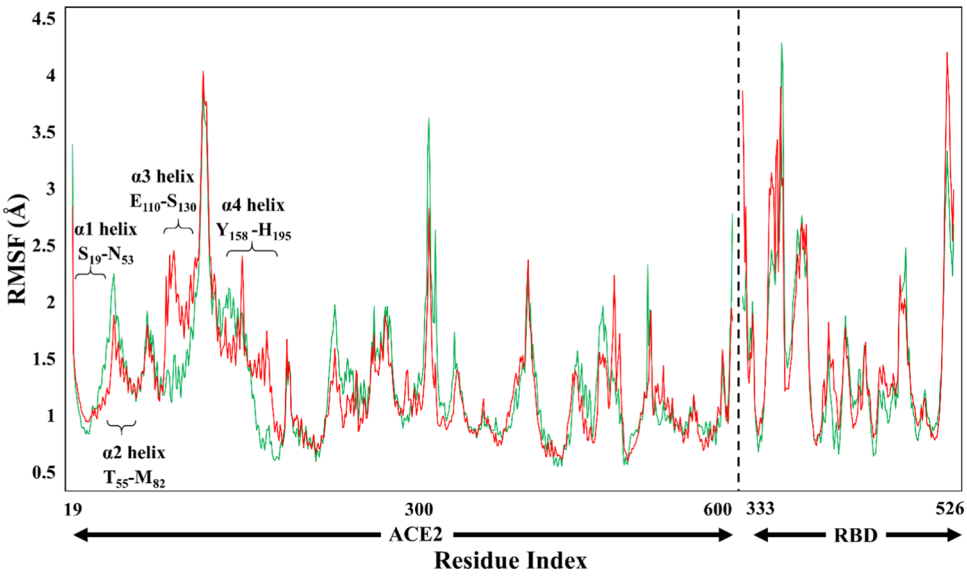

Figure 4. Root-mean-square fluctuations (RMSFs) of the $\mathbf{RA_O}$ (green) and $\mathbf{RA'_O}$ (red) complexes.

on the RMSF and porcupine plot of the complexes (Figures 4 and S10). Subdomain I is composed of the α1 (S19−N53) and α2 (T55−M82) helices and subdomain II contains the α3 (E110−G130) and α4 (Y158−H195) helices (see Figure 5).

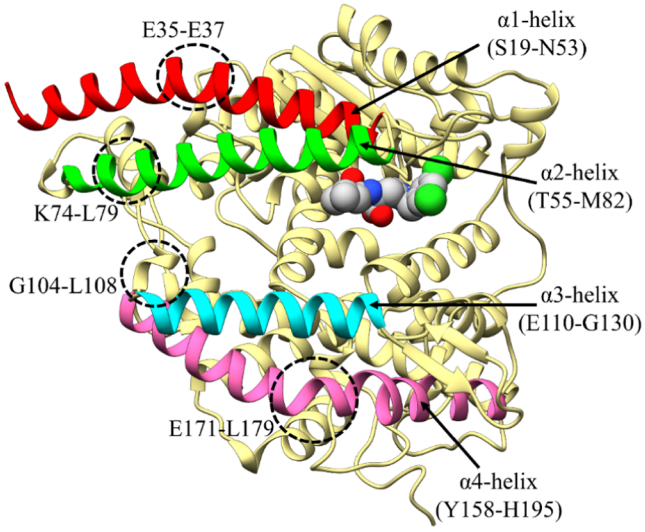

Figure 5. Fluctuations observed in the ACE2 enzyme.

Even though the complex fluctuates during the simulation, the overall structure of the $\mathbf{RA'_O}$ complex remained the same, i.e., ACE2 in the open conformation. Similarly, Kobophenol A also shows minor fluctuations in the ACE2 enzyme and the overall ACE2−RBD complex structure remained the same.[51] A superposition of the equilibrated (red) and X-ray (blue) structures showed a minor displacement of residues in the α3 helix, which is highlighted with yellow arrows in Figure S11. On the other hand, in the $\mathbf{RA_O}$ complex, in the absence of an inhibitor, ACE2 becomes partially closed (Figure 3A). The yellow arrows on the superposition of the most representative (red) and X-ray (blue) structures display the partial closing of the ACE2 receptor (RMSD = 2.2 Å) (Figure S11C).

In addition, the superposition of the $\mathbf{RA_O}$ and $\mathbf{RA'_O}$ models showed a structural difference between these two complexes with an RMSD of 2.4 Å (see Figure S11A). Another difference between the two complexes was detected in the RMSF graph indicating a difference in fluctuation in the α3 and α4 helix (labeled in Figure 4). The partial differences between the two complexes ($\mathbf{RA_O}$ and $\mathbf{RA'_O}$) could be related to the binding of the MLN-4760 inhibitor to the ACE2 enzyme. In the MD simulations, multiple second coordination shell residues get reoriented upon inhibitor binding, stabilizing the ACE2−inhibitor complex either through direct or water-mediated noncovalent interactions. These interacting residues are shown in Figure 2. As discussed in Section 3, in the $\mathbf{A'_C}$ complex, the presence of an inhibitor causes an opening of the ACE2 flaps during the simulation. A reasonably clear distinction can be made between its open and closed structures, as shown in Figure S10. The RMSD obtained by the superposition of these two structures ($\mathbf{A'_{C1}}$ and $\mathbf{A'_{C2}}$) was 3.7 Å. On the other hand, in the $\mathbf{A_C}$ complex, the ACE2 receptor remains closed during the entire simulation. Similarly, in the $\mathbf{A_O}$ and $\mathbf{A'_O}$ complexes, the structure of the ACE2 receptor remains open. The computed RMSD values with their respective X-ray structures were quite low, i.e., 2.8, 2.5, 2.3, and 2.4 Å for $\mathbf{A_O}$, $\mathbf{A_C}$, $\mathbf{A'_O}$, and $\mathbf{A'_C}$, respectively. All of the evidence suggests that the inhibitor tends to open the ACE2 complex, while the absence results in its closure or partial closure.

3.3. ACE2−RBD Interface Interactions. The binding of RBD to ACE2 is a crucial step in the entry of the coronavirus to the epithelial cell.[15] The binding affinity of SARS-CoV-2 to ACE2 is ∼10 to ∼20 times higher in comparison to SARS-CoV[10] and could be one of the many factors contributing to the worldwide spreading of the disease. These strong interactions are mediated mainly through electrostatic complementarity, hydrogen bonding, and hydrophobic interactions, as suggested by hydrophobic surface maps (Figure S4). The RBD interacts mainly through the α helix (α1 and α2) and loops (I and II) of the ACE2 receptor (Figure 3). Overall, in the $\mathbf{RA_O}$ complex, 25 hydrogen bonds and four CH−π interactions were observed at the interface, while at the $\mathbf{RA'_O}$ interface, 24 hydrogen bonds and three CH−π interactions were detected (see Table 1). Major changes in the interactions were recognized only in the α1 helix, while on the α2 helix and loop I, the interactions were almost the same. On the α1 helix, 13 interactions (i.e., 11 hydrogen bonds

https://doi.org/10.1021/acs.jcim.1c01283
J. Chem. Inf. Model. XXXX, XXX, XXX−XXX

Table 1. Hydrogen Bonds and CH−π Interactions (in Å) between the ACE2 and Inhibitor

	RA_O	H-Bond (Å)	RA'_O	H-bond (Å)
α1 helix	S19−S477	3.00, 3.35		
	Q24−A475	2.00	Q24−A475	2.11
			Q24−G476	2.87
			D30−K417	1.77
			K31−Q493	1.78
	H34−Q493	2.25	H34−Q493	2.70
	E35−Q493	1.90	E35−Q493	1.97
	E37−Y505	1.78, 2.62		
	D38−Y449	1.62		
	D38−Q498	1.78	D38−Q498	2.00
	Y41−T500	2.27, 2.72	Y41−T500	2.92, 2.73
α2 helix	Y83−N487	1.66	Y83−N487	2.02
Loop I	K353−G496	2.42, 2.96, 2.92	K353−G496	2.78, 2.72, 2.84
	K353−Q498	1.99, 2.97	K353−Q498	1.93, 2.90,
	K353−N501	2.64	K353−N501	2.45
	K353−Y495	2.09	K353−Y495	2.11
	K353−G502	1.95	K353−G502	1.97
	D355−T500	2.08	D355−T500	1.71, 3.35
	R357−T500	2.29, 3.34	R357−T500	2.54, 2.97
	R393−Y505	2.78, 3.03	R393−Y505	3.08, 3.43
		CH−π (Å)		CH−π (Å)
α2 helix	M82−F486	3.5	M82−F498	2.7
	Y83−F486	2.5	Y83−F486	3.3
Loop II	K31−Y489	3.0	K31−Y489	3.0
	H34−L455	3.0		

and two CH−π interactions) were observed in the RA_O complex, while only 10 interactions (i.e., nine hydrogen bonds and one CH−π interaction) were detected in the RA'_O complex. On the α1 helix of the RA'_O complex, hydrogen-bond interactions between S19−S477, E37−Y505, and D38−Y449 were lost during the simulation, while new interactions between Q24−G476, D30−K417, and K31−Q493 were formed. The change in the residue interactions is assumed to be due to the opening and partial closing of the ACE2 receptor. In both the RA_O and RA'_O complexes, the α2 helix formed only one hydrogen-bond (Y83−N487) and two CH−π interactions (M82−F486 and Y83−F486) with the RBD. Similarly, on loop II, the number of interactions in both complexes remained the same.

In summary, our calculations highlighted that the hydrogen-bond interactions in both complexes played an essential role in stabilizing the binding conformation. However, the fluctuations caused by the inhibitor did not display a major effect on the interface binding as the number of hydrogen bonds remains nearly the same.

3.4. Fluctuations in the RBD. The bending motion detected upon inhibitor binding occurs as subdomain I moves to close the gap and in doing so brings critical residue groups into contact with the substrate/inhibitor. Even after fluctuations in the ACE2 due to this inhibitor, almost no fluctuation in the RBD was observed. A superimposition of the two RBD did not show a major change in the structure. However, the protein's secondary structure analysis revealed changes in the E340−A344 and V367−S375 residues due to the loss of the α-helical property (Figure S13).

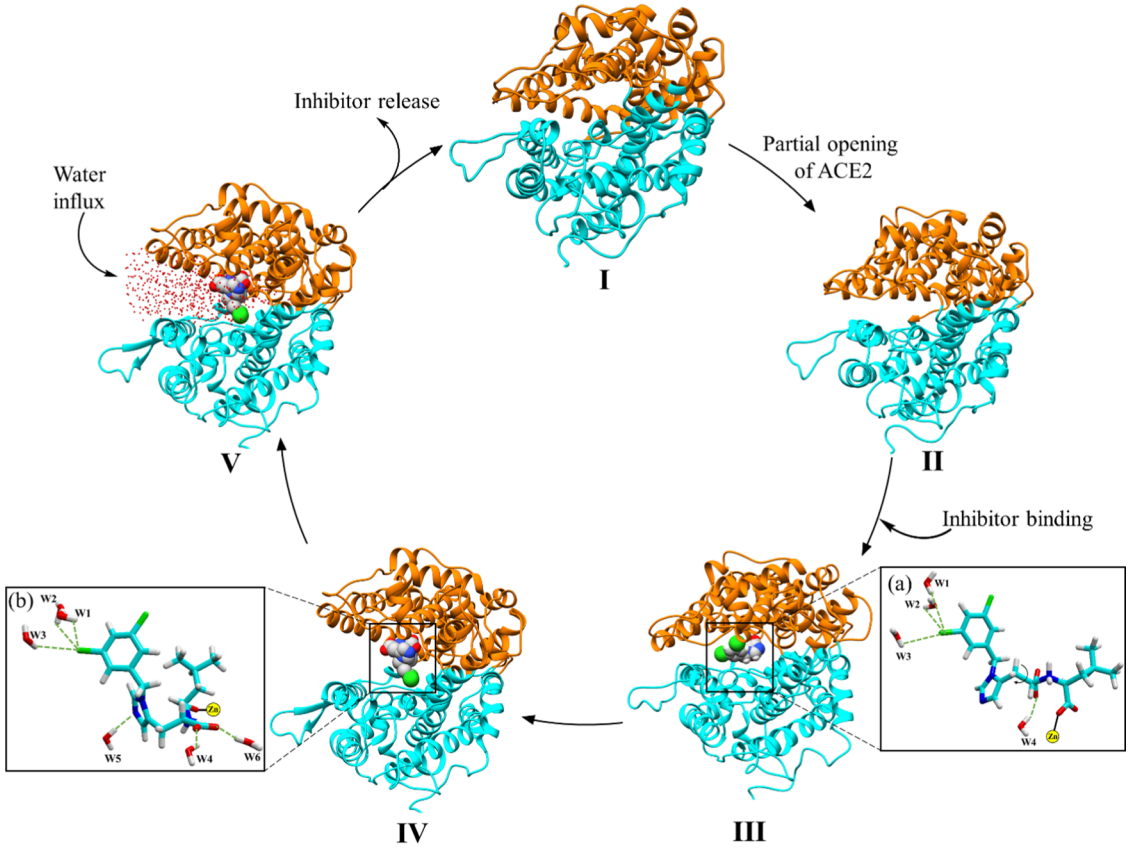

Figure 6. Opening and closing mechanisms of ACE2.

https://doi.org/10.1021/acs.jcim.1c01283
J. Chem. Inf. Model. XXXX, XXX, XXX−XXX

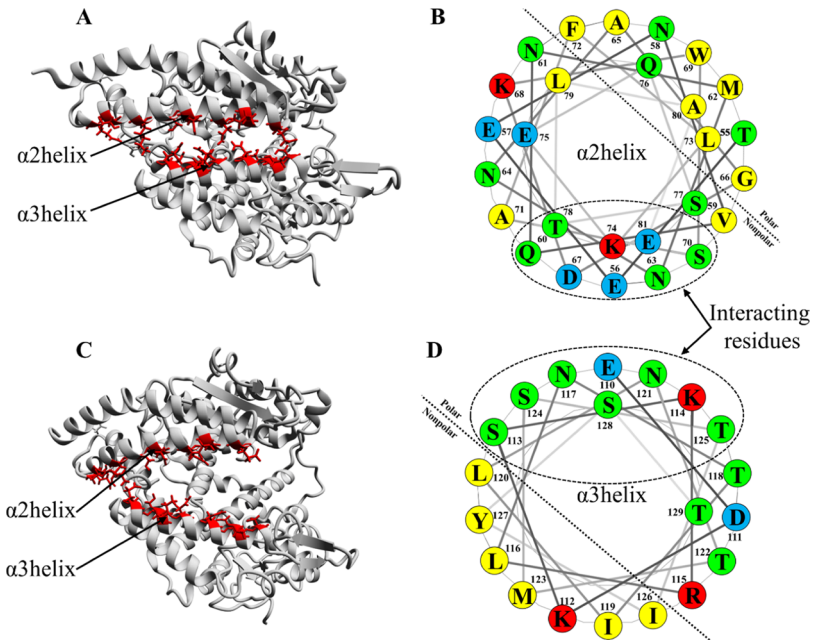

Figure 7. (A, C) ACE2 in closed and open conformations, respectively. The polar residues on the $\alpha 2$ helix (red color) interact with the polar residues on the $\alpha 3$ helix (red color) via hydrogen bonds; (B, D) helical wheel projection of the $\alpha 2$ and $\alpha 3$ helix, respectively. The interacting polar residues are shown in the dotted circle.

3.5. Opening and Closing Mechanisms of ACE2. The opening/closing dynamics of ACE2 are characterized by the distance between $\alpha 2$ and $\alpha 3$ helices (i.e., if they are far it is in the open conformation and if they are close it is in the closed conformation). The proposed ACE2 opening and closing mechanisms are as follows: initially, in an inactive state, the ACE2 is in a closed form with few water molecules trapped inside the active site cavity (**I** in Figure 6). In the presence of a substrate/inhibitor, the ACE2 enzyme partially opens, allowing access to the active site (**II** in Figure 6). Figure S7 shows that the binding of the substrate/inhibitor can only take place in the open conformation of the ACE2 enzyme since in the closed conformation the active site is inaccessible. In the next step, the substrate/inhibitor binds to the Zn ion of the active site (**III** in Figure 6). Consequently, the substrate undergoes catalytic hydrolysis and leaves the active site cleft. Finally, the polar residues on the $\alpha 2$ and $\alpha 3$ helices come close and switch the gate to a shut state and arrest the enzyme in its closed, inactive conformation (see Figures 7 and S12). On the other hand, the inhibitor will remain bound to the metal ion inactivating ACE2. The inhibitor−solvent interaction causes the torsional rotation of the imidazole ring and carboxylate group at the C−C bond (**IV** in Figure 6), which forms a V shape structure and assists the inhibitor to interact with subdomain II (Figure 6a,b). Simultaneously, the opening of the ACE2 enzyme also causes the water molecule to enter the cleft allowing higher substrate/inhibitor−solvent interactions (**V** in Figure 6). A similar flexible/breathing motion has also been suggested to allow substrate binding in the ACE1 enzyme.[17] In all simulations, a bending motion (fluctuations) was observed at four regions (circled in Figure 5), i.e., (a) $\alpha 1$ helix (at E35−E37); (b) $\alpha 2$ helix (at K74−L79); (c) $\alpha 3$ helix (at G104−L108); and (d) $\alpha 4$ helix (at E171−L179). Due to these fluctuations, a distinct change in the secondary structure of the ACE2 enzyme was detected. Fluctuation in these four sites may be crucial for the opening and closing of the ACE2 enzyme. To obtain further insights into the dynamic behavior of the helices, we monitored the secondary protein structure, which shows that the overall secondary structure was lost at these specific locations (see Figure S13).

Additionally, to the above-mentioned fluctuations in ACE2, the opening/closing mechanism also depends on the interaction between the $\alpha 2$ and $\alpha 3$ helix. The polar residues on the two helices are facing each other, which facilitate interactions with the two anionic surfaces and help in the opening and closing of the ACE2 clamp by forming direct or water-mediated hydrogen-bond interactions. The helical wheel projection of the $\alpha 2$ and $\alpha 3$ helix displaying its amphipathic character is shown in Figure 7. Based on the results, we propose that the distribution of polar amino acid residues on one side of the helix is an important parameter for the clamshell mechanism of ACE2. Although further molecular analysis is required to establish a full angiotensin II binding and cleavage cycle, the open and closure of ACE2 in the present analysis already indicate that a significant conformational change is required for the inhibition activity of the ACE2 enzyme.

5. CONCLUSIONS

In the present MD simulation study, molecular interaction between the SARS-CoV-2 S protein RBD and ACE2 receptor has been investigated. In addition, the role of the inhibitor on the dynamic transformation of the ACE2 and RBD and their interface has been elucidated. According to our MD simulations, the process is initiated by the binding of a potent ACE2 inhibitor (MLN-4760) to the ACE2 receptor active site. To accommodate the inhibitor, the ACE2 receptor should be in an open state. The binding is driven by interactions with the positively charged Zn^{2+} ion and second coordination shell residues present in the active site. The most representative structure of the complexes show that the chemical nature of the inhibitor causes fluctuations in the surrounding residues causing different conformational dynamics in both $\mathbf{RA_O}$ and $\mathbf{RA'_O}$ complexes. The presence of an inhibitor tends to open the ACE2 receptor

https://doi.org/10.1021/acs.jcim.1c01283
J. Chem. Inf. Model. XXXX, XXX, XXX−XXX

where the two subdomains (**I** and **II**) move away from each other, while the absence results in partial closure. These results were supported by the RMSF, the secondary structure of the protein, and porcupine plots. Furthermore, the difference in the angle of the ACE2 clam, caused by the shrinking of the distance between $\alpha 2$ and $\alpha 3$, explicitly indicated the flexibility of the helices. Although our MD simulations supported the role of the inhibitor in the modification of ACE2 structures, it does not demonstrate major changes in the coordination interactions between ACE2 and RBD. The number of hydrogen-bond interactions on their interface remains the same, i.e., 25 and 23, in $\mathbf{RA_O}$ and $\mathbf{RA'_O}$, respectively. Clarification of the structure−function relationship of the ACE2 and ACE2−RBD complex will not only facilitate the understanding of the ACE2 enzyme and its interactions with RBD but also aid in drug discovery of the ACE2 inhibitors against coronavirus.

■ ASSOCIATED CONTENT

Supporting Information

The Supporting Information is available free of charge at https://pubs.acs.org/doi/10.1021/acs.jcim.1c01283.

Secondary structure evolution, insertion depth profiles, and additional experimental details for all simulation trials (Figures S1−S13) (PDF)

(PDF)

■ AUTHOR INFORMATION

Corresponding Author

Kenneth M. Merz − *Department of Chemistry, Michigan State University, East Lansing, Michigan 48824, United States; Department of Biochemistry and Molecular Biology, Michigan State University, East Lansing, Michigan 48824, United States;* orcid.org/0000-0001-9139-5893; Phone: (517) 355-9715; Email: merz@chemistry.msu.edu

Authors

Gaurav Sharma − *Department of Chemistry, Michigan State University, East Lansing, Michigan 48824, United States;* orcid.org/0000-0002-1031-5378

Lin Frank Song − *Department of Chemistry, Michigan State University, East Lansing, Michigan 48824, United States*

Complete contact information is available at: https://pubs.acs.org/10.1021/acs.jcim.1c01283

Funding

This work was supported in part by an NIH grant (award number GM130641).

Notes

The authors declare no competing financial interest.

Requirements for existing software apply to this manuscript: software used for MD simulations is AMBER18 available at http://ambermd.org/. The ACE2−inhibitor 2D interaction graph was prepared by Schrodinger suite 2019-4, provided by the high-performance computer center (iCER HPCC) at Michigan State University. The helical wheel projection of $\alpha 2$ and $\alpha 3$ helices of the ACE2 receptor was obtained from the NetWheel online web server at http://lbqp.unb.br/NetWheels. The restart and topology files are freely accessible at https://github.com/gauravsharmamsu/COVID_Research.git. Given their large dimensions, full trajectories are available upon request.

■ ACKNOWLEDGMENTS

The authors of this manuscript are committed to supporting and advancing women in chemistry. This work was supported in part by NIH grant number GM130641. The authors are grateful to the Department of Chemistry and Biochemistry and the high-performance computer center (iCER HPCC) at Michigan State University.

■ ABBREVIATIONS

RBD, receptor-binding domain; PD, peptidase domain; ACE2, angiotensin-converting enzyme 2

■ REFERENCES

(1) Hui, D. S.; Azhar, E. I.; Madani, T. A.; Ntoumi, F.; Kock, R.; Dar, O.; Ippolito, G.; Mchugh, T. D.; Memish, Z. A.; Drosten, C.; et al. The continuing 2019-nCoV epidemic threat of novel coronaviruses to global health—The latest 2019 novel coronavirus outbreak in Wuhan, China. *Int. J. Infect. Dis.* **2020**, *91*, 264−266.

(2) Zhong, N.; Zheng, B.; Li, Y.; Poon, L.; Xie, Z.; Chan, K.; Li, P.; Tan, S.; Chang, Q.; Xie, J.; et al. Epidemiology and cause of severe acute respiratory syndrome (SARS) in Guangdong, People's Republic of China, in February, 2003. *Lancet* **2003**, *362*, 1353−1358.

(3) de Groot, R. J.; Baker, S. C.; Baric, R. S.; Brown, C. S.; Drosten, C.; Enjuanes, L.; Fouchier, R. A.; Galiano, M.; Gorbalenya, A. E.; Memish, Z. A.; et al. Commentary: Middle east respiratory syndrome coronavirus (mers-cov): announcement of the coronavirus study group. *J. Virol.* **2013**, *87*, 7790−7792.

(4) Mahase, E. British Medical Journal Publishing Group, 2020.

(5) Lan, J.; Ge, J.; Yu, J.; Shan, S.; Zhou, H.; Fan, S.; Zhang, Q.; Shi, X.; Wang, Q.; Zhang, L.; Wang, X. Structure of the SARS-CoV-2 spike receptor-binding domain bound to the ACE2 receptor. *Nature* **2020**, *581*, 215−220.

(6) Towler, P.; Staker, B.; Prasad, S. G.; Menon, S.; Tang, J.; Parsons, T.; Ryan, D.; Fisher, M.; Williams, D.; Dales, N. A.; et al. ACE2 X-ray structures reveal a large hinge-bending motion important for inhibitor binding and catalysis. *J. Biol. Chem.* **2004**, *279*, 17996−18007.

(7) Guy, J. L.; Jackson, R. M.; Jensen, H. A.; Hooper, N. M.; Turner, A. J. Identification of critical active-site residues in angiotensin-converting enzyme-2 (ACE2) by site-directed mutagenesis. The. *FEBS J.* **2005**, *272*, 3512−3520.

(8) Kirchdoerfer, R. N.; Cottrell, C. A.; Wang, N.; Pallesen, J.; Yassine, H. M.; Turner, H. L.; Corbett, K. S.; Graham, B. S.; McLellan, J. S.; Ward, A. B. Pre-fusion structure of a human coronavirus spike protein. *Nature* **2016**, *531*, 118−121.

(9) Lu, R.; Zhao, X.; Li, J.; Niu, P.; Yang, B.; Wu, H.; Wang, W.; Song, H.; Huang, B.; Zhu, N.; et al. Genomic characterisation and epidemiology of 2019 novel coronavirus: implications for virus origins and receptor binding. *Lancet* **2020**, *395*, 565−574.

(10) Wrapp, D.; Wang, N.; Corbett, K. S.; Goldsmith, J. A.; Hsieh, C.-L.; Abiona, O.; Graham, B. S.; McLellan, J. S. Cryo-EM structure of the 2019-nCoV spike in the prefusion conformation. *Science* **2020**, *367*, 1260−1263.

(11) Shang, J.; Ye, G.; Shi, K.; Wan, Y.; Luo, C.; Aihara, H.; Geng, Q.; Auerbach, A.; Li, F. Structural basis of receptor recognition by SARS-CoV-2. *Nature* **2020**, 221−224.

(12) Tai, W.; He, L.; Zhang, X.; Pu, J.; Voronin, D.; Jiang, S.; Zhou, Y.; Du, L. Characterization of the receptor-binding domain (RBD) of 2019 novel coronavirus: implication for development of RBD protein as a viral attachment inhibitor and vaccine. *Cell. Mol. Immunol.* **2020**, 613−620.

(13) Spinello, A.; Saltalamacchia, A.; Magistrato, A. Is the Rigidity of SARS-CoV-2 Spike Receptor-Binding Motif the Hallmark for Its Enhanced Infectivity? Insights from All-Atoms Simulations. *J. Phys. Chem. Lett.* **2020**, 4785−4790.

(14) Walls, A. C.; Park, Y.-J.; Tortorici, M. A.; Wall, A.; McGuire, A. T.; Veesler, D. Structure, function, and antigenicity of the SARS-CoV-2 spike glycoprotein. *Cell* **2020**, 281−292.e6.

(15) Tian, X.; Li, C.; Huang, A.; Xia, S.; Lu, S.; Shi, Z.; Lu, L.; Jiang, S.; Yang, Z.; Wu, Y.; Ying, T. Potent binding of 2019 novel coronavirus spike protein by a SARS coronavirus-specific human monoclonal antibody. *Emerging Microbes Infect.* **2020**, *9*, 382−385.
(16) Sanders, J. M.; Monogue, M. L.; Jodlowski, T. Z.; Cutrell, J. B. Pharmacologic treatments for coronavirus disease 2019 (COVID-19): a review. *Jama* **2020**, *323*, 1824−1836.
(17) Siddiqi, H. K.; Mehra, M. R. COVID-19 illness in native and immunosuppressed states: A clinical−therapeutic staging proposal. *J. Heart Lung Transplant.* **2020**, *39*, 405.
(18) Wang, X.; Guo, X.; Xin, Q.; Pan, Y.; Hu, Y.; Li, J.; Chu, Y.; Feng, Y.; Wang, Q. Neutralizing antibodies responses to SARS-CoV-2 in COVID-19 inpatients and convalescent patients. *Clin. Infect. Dis.* **2020**, 2688−2694.
(19) Mair-Jenkins, J.; Saavedra-Campos, M.; Baillie, J. K.; Cleary, P.; Khaw, F.-M.; Lim, W. S.; Makki, S.; Rooney, K. D.; Group, C. P. S.; Nguyen-Van-Tam, J. S. The effectiveness of convalescent plasma and hyperimmune immunoglobulin for the treatment of severe acute respiratory infections of viral etiology: a systematic review and exploratory meta-analysis. *J. Infect. Dis.* **2015**, *211*, 80−90.
(20) Zhong, J.; Tang, J.; Ye, C.; Dong, L. The immunology of COVID-19: is immune modulation an option for treatment? *Lancet Rheumatol.* **2020**, e428−e436.
(21) Horby, P.; Lim, W.; Emberson, J.; Mafham, M.; Bell, J.; Linsell, L.; Staplin, N.; Brightling, C.; Ustianowski, A.; Elmahi, E. Effect of dexamethasone in hospitalized patients with COVID-19: preliminary report. *medRxiv* **2020**, 22.
(22) Jin, Z.; Zhao, Y.; Sun, Y.; Zhang, B.; Wang, H.; Wu, Y.; Zhu, Y.; Zhu, C.; Hu, T.; Du, X.; et al. Structural basis for the inhibition of SARS-CoV-2 main protease by antineoplastic drug carmofur. *Nat. Struct. Mol. Biol.* **2020**, *27*, 529−532.
(23) Ghosh, A. K.; Xi, K.; Grum-Tokars, V.; Xu, X.; Ratia, K.; Fu, W.; Houser, K. V.; Baker, S. C.; Johnson, M. E.; Mesecar, A. D. Structure-based design, synthesis, and biological evaluation of peptidomimetic SARS-CoV 3CLpro inhibitors. *Bioorg. Med. Chem. Lett.* **2007**, *17*, 5876−5880.
(24) Liu, Y.; Liang, C.; Xin, L.; Ren, X.; Tian, L.; Ju, X.; Li, H.; Wang, Y.; Zhao, Q.; Liu, H.; et al. The development of Coronavirus 3C-Like protease (3CLpro) inhibitors from 2010 to 2020. *Eur. J. Med. Chem.* **2020**, No. 112711.
(25) Ragia, G.; Manolopoulos, V. G. Inhibition of SARS-CoV-2 entry through the ACE2/TMPRSS2 pathway: a promising approach for uncovering early COVID-19 drug therapies. *Eur. J. Clin. Pharmacol.* **2020**, 1623−1630.
(26) Ryu, W.-S. Virus Life Cycle. In *Molecular Virology of Human Pathogenic*; Academic Press, 2017; pp 31−45.
(27) Gulick, R. M.; Lalezari, J.; Goodrich, J.; Clumeck, N.; DeJesus, E.; Horban, A.; Nadler, J.; Clotet, B.; Karlsson, A.; Wohlfeiler, M.; et al. Maraviroc for previously treated patients with R5 HIV-1 infection. *N. Engl. J. Med.* **2008**, *359*, 1429−1441.
(28) Chi, X.; Yan, R.; Zhang, J.; Zhang, G.; Zhang, Y.; Hao, M.; Zhang, Z.; Fan, P.; Dong, Y.; Yang, Y.; et al. A neutralizing human antibody binds to the N-terminal domain of the Spike protein of SARS-CoV-2. *Science* **2020**, *369*, 650−655.
(29) Baum, A.; Fulton, B. O.; Wloga, E.; Copin, R.; Pascal, K. E.; Russo, V.; Giordano, S.; Lanza, K.; Negron, N.; Ni, M.; et al. Antibody cocktail to SARS-CoV-2 spike protein prevents rapid mutational escape seen with individual antibodies. *Science* **2020**, *369*, 1014−1018.
(30) Chen, X.; Li, R.; Pan, Z.; Qian, C.; Yang, Y.; You, R.; Zhao, J.; Liu, P.; Gao, L.; Li, Z.; et al. Human monoclonal antibodies block the binding of SARS-CoV-2 spike protein to angiotensin converting enzyme 2 receptor. *Cell. Mol. Immunol.* **2020**, 647−649.
(31) Xiang, Z.; Liu, J.; Shi, D.; Chen, W.; Li, J.; Yan, R.; Bi, Y.; Hu, W.; Zhu, Z.; Yu, Y.; Yang, Z. Glucocorticoids improve severe or critical COVID-19 by activating ACE2 and reducing IL-6 levels. *Int. J. Biol. Sci.* **2020**, *16*, 2382−2391.
(32) Ghahremanpour, M. M.; Tirado-Rives, J.; Deshmukh, M.; Ippolito, J. A.; Zhang, C.-H.; de Vaca, I. C.; Liosi, M.-E.; Anderson, K. S.; Jorgensen, W. L. Identification of 14 Known Drugs as Inhibitors of the Main Protease of SARS-CoV-2. *ACS Med. Chem. Lett.* **2020**, 2526−2533.
(33) Zhou, Y.; Hou, Y.; Shen, J.; Huang, Y.; Martin, W.; Cheng, F. Network-based drug repurposing for novel coronavirus 2019-nCoV/SARS-CoV-2. *Cell Discovery* **2020**, *6*, 1−18.
(34) Santos, R.; Ursu, O.; Gaulton, A.; Bento, A. P.; Donadi, R. S.; Bologa, C. G.; Karlsson, A.; Al-Lazikani, B.; Hersey, A.; Oprea, T. I.; Overington, J. P. A comprehensive map of molecular drug targets. *Nat. Rev. Drug Discovery* **2017**, *16*, 19−34.
(35) Touret, F.; Gilles, M.; Barral, K.; Nougairède, A.; van Helden, J.; Decroly, E.; de Lamballerie, X.; Coutard, B. In vitro screening of a FDA approved chemical library reveals potential inhibitors of SARS-CoV-2 replication. *Sci. Rep.* **2020**, *10*, No. 13093.
(36) Muratov, E. N.; Amaro, R.; Andrade, C. H.; Brown, N.; Ekins, S.; Fourches, D.; Isayev, O.; Kozakov, D.; Medina-Franco, J. L.; Merz, K. M.; et al. A critical overview of computational approaches employed for COVID-19 drug discovery. *Chem. Soc. Rev.* **2021**, 9121−9151.
(37) Li, X.; Yu, J.; Zhang, Z.; Ren, J.; Peluffo, A. E.; Zhang, W.; Zhao, Y.; Wu, J.; Yan, K.; Cohen, D.; Wang, W. Network bioinformatics analysis provides insight into drug repurposing for COVID-19. *Med. Drug Discovery* **2021**, *10*, No. 100090.
(38) Galindez, G.; Matschinske, J.; Rose, T. D.; Sadegh, S.; Salgado-Albarrán, M.; Späth, J.; Baumbach, J.; Pauling, J. K. Lessons from the COVID-19 pandemic for advancing computational drug repurposing strategies. *Nat. Comput. Sci.* **2021**, *1*, 33−41.
(39) Su, H.; Zhou, F.; Huang, Z.; Ma, X.; Natarajan, K.; Zhang, M.; Huang, Y.; Su, H. Molecular Insights into Small-Molecule Drug Discovery for SARS-CoV-2. *Angew. Chem.* **2021**, *133*, 9873−9886.
(40) Pushpakom, S.; Iorio, F.; Eyers, P. A.; Escott, K. J.; Hopper, S.; Wells, A.; Doig, A.; Guilliams, T.; Latimer, J.; McNamee, C.; et al. Drug repurposing: progress, challenges and recommendations. *Nat. Rev. Drug Discovery* **2019**, *18*, 41−58.
(41) Corsello, S. M.; Bittker, J. A.; Liu, Z.; Gould, J.; McCarren, P.; Hirschman, J. E.; Johnston, S. E.; Vrcic, A.; Wong, B.; Khan, M.; et al. The Drug Repurposing Hub: a next-generation drug library and information resource. *Nat. Med.* **2017**, *23*, 405−408.
(42) Choudhary, S.; Malik, Y. S.; Tomar, S. Identification of SARS-CoV-2 cell entry inhibitors by drug repurposing using in silico structure-based virtual screening approach. *Front. Immunol.* **2020**, *11*, No. 1664.
(43) Maffucci, I.; Contini, A. In Silico Drug Repurposing for SARS-CoV-2 Main Proteinase and Spike Proteins. *J. Proteome Res.* **2020**, 4637−4648.
(44) Trezza, A.; Iovinelli, D.; Santucci, A.; Prischi, F.; Spiga, O. An integrated drug repurposing strategy for the rapid identification of potential SARS-CoV-2 viral inhibitors. *Sci. Rep.* **2020**, *10*, No. 13866.
(45) Gutierrez-Villagomez, J. M.; Campos-García, T.; Molina-Torres, J.; López, M. G.; Vázquez-Martínez, J. Alkamides and piperamides as potential antivirals against the severe acute respiratory syndrome coronavirus 2 (SARS-CoV-2). *J. Phys. Chem. Lett.* **2020**, *11*, 8008−8016.
(46) Panda, S. K.; Gupta, P. S. S.; Biswal, S.; Ray, A. K.; Rana, M. K. ACE-2-derived Biomimetic Peptides for the Inhibition of Spike Protein of SARS-CoV-2. *J. Proteome Res.* **2020**, 1296−1303.
(47) Huang, X.; Pearce, R.; Zhang, Y. Computational design of peptides to block binding of the SARS-CoV-2 spike protein to human ACE2. *BioRxiv* **2020**, DOI: 10.1101/2020.03.28.013607.
(48) Han, Y.; Král, P. Computational design of ACE2-based short peptide inhibitors of SARS-CoV-2. *ACS Nano* **2020**, 5143−5147.
(49) Pandey, P.; Chatterjee, S.; Berida, T.; Doerksen, R. J.; Roy, S. Targeting SARS-CoV-2 spike protein of COVID-19 with naturally occurring phytochemicals: an in silico study for drug development. *J. Biomol. Struct. Dyn.* **2020**, 1−18.
(50) Chen, H.; Du, Q. Potential natural compounds for preventing SARS-CoV-2 (2019-nCoV) infection. Preprints 2020.
(51) Gangadevi, S.; Badavath, V. N.; Thakur, A.; Yin, N.; De Jonghe, S.; Acevedo, O.; Jochmans, D.; Leyssen, P.; Wang, K.; Neyts, J.; et al. Kobophenol A Inhibits Binding of Host ACE2 Receptor with Spike

RBD Domain of SARS-CoV-2, a Lead Compound for Blocking COVID-19. *J. Phys. Chem. Lett.* **2021**, *12*, 1793−1802.

(52) Mesli, F.; Ghalem, M.; Daoud, I.; Ghalem, S. Potential inhibitors of angiotensin converting enzyme 2 receptor of COVID-19 by Corchorus olitorius Linn using docking, molecular dynamics, conceptual DFT investigation and pharmacophore mapping. *J. Biomol. Struct. Dyn.* **2021**, 1−13.

(53) Walsh, E. E.; Frenck, R. W., Jr.; Falsey, A. R.; Kitchin, N.; Absalon, J.; Gurtman, A.; Lockhart, S.; Neuzil, K.; Mulligan, M. J.; Bailey, R.; et al. Safety and immunogenicity of two RNA-based Covid-19 vaccine candidates. *N. Engl. J. Med.* **2020**, *383*, 2439−2450.

(54) Polack, F. P.; Thomas, S. J.; Kitchin, N.; Absalon, J.; Gurtman, A.; Lockhart, S.; Perez, J. L.; Pérez Marc, G.; Moreira, E. D.; Zerbini, C.; et al. Safety and efficacy of the BNT162b2 mRNA Covid-19 vaccine. *N. Engl. J. Med.* **2020**, *383*, 2603−2615.

(55) Chagla, Z. The BNT162b2 (BioNTech/Pfizer) vaccine had 95% efficacy against COVID-19≥ 7 days after the 2nd dose. *Ann. Intern. Med.* **2021**, *174*, JC15.

(56) Voysey, M.; Clemens, S. A. C.; Madhi, S. A.; Weckx, L. Y.; Folegatti, P. M.; Aley, P. K.; Angus, B.; Baillie, V. L.; Barnabas, S. L.; Bhorat, Q. E.; et al. Single-dose administration and the influence of the timing of the booster dose on immunogenicity and efficacy of ChAdOx1 nCoV-19 (AZD1222) vaccine: a pooled analysis of four randomised trials. *Lancet* **2021**, *397*, 881−891.

(57) Knoll, M. D.; Wonodi, C. Oxford−AstraZeneca COVID-19 vaccine efficacy. *Lancet* **2021**, *397*, 72−74.

(58) Oliver, S. E.; Gargano, J. W.; Scobie, H.; Wallace, M.; Hadler, S. C.; Leung, J.; Blain, A. E.; McClung, N.; Campos-Outcalt, D.; Morgan, R. L.; et al. The Advisory Committee on Immunization Practices' Interim Recommendation for Use of Janssen COVID-19 Vaccine—United States, February 2021. *MMWR Morb. Mortal. Wkly. Rep.* **2021**, *70*, 329.

(59) Zhang, Y.; Zeng, G.; Pan, H.; Li, C.; Hu, Y.; Chu, K.; Han, W.; Chen, Z.; Tang, R.; Yin, W.; et al. Safety, tolerability, and immunogenicity of an inactivated SARS-CoV-2 vaccine in healthy adults aged 18−59 years: a randomised, double-blind, placebo-controlled, phase 1/2 clinical trial. *Lancet Infect. Dis.* **2021**, *21*, 181−192.

(60) Xia, S.; Zhang, Y.; Wang, Y.; Wang, H.; Yang, Y.; Gao, G. F.; Tan, W.; Wu, G.; Xu, M.; Lou, Z.; et al. Safety and immunogenicity of an inactivated SARS-CoV-2 vaccine, BBIBP-CorV: a randomised, double-blind, placebo-controlled, phase 1/2 trial. *Lancet Infect. Dis.* **2021**, *21*, 39−51.

(61) Kamal, D.; Thakur, V.; Nath, N.; Malhotra, T.; Gupta, A.; Batlish, R. Adverse events following ChAdOx1 nCoV-19 Vaccine (COVISHIELD) amongst health care workers: A prospective observational study. *Med. J. Armed Forces India* **2021**, *77*, S283−S288.

(62) Tipnis, S. R.; Hooper, N. M.; Hyde, R.; Karran, E.; Christie, G.; Turner, A. J. A human homolog of angiotensin-converting enzyme cloning and functional expression as a captopril-insensitive carboxypeptidase. *J. Biol. Chem.* **2000**, *275*, 33238−33243.

(63) Douglas, G. C.; O'Bryan, M. K.; Hedger, M. P.; Lee, D. K.; Yarski, M. A.; Smith, A. I.; Lew, R. A. The novel angiotensin-converting enzyme (ACE) homolog, ACE2, is selectively expressed by adult Leydig cells of the testis. *Endocrinology* **2004**, *145*, 4703−4711.

(64) Skeggs, L. T., Jr; Kahn, J. R.; Shumway, N. P. The preparation and function of the hypertensin-converting enzyme. *J. Exp. Med.* **1956**, *103*, No. 295.

(65) Dales, N. A.; Gould, A. E.; Brown, J. A.; Calderwood, E. F.; Guan, B.; Minor, C. A.; Gavin, J. M.; Hales, P.; Kaushik, V. K.; Stewart, M.; et al. Substrate-based design of the first class of angiotensin-converting enzyme-related carboxypeptidase (ACE2) inhibitors. *J. Am. Chem. Soc.* **2002**, *124*, 11852−11853.

(66) Mores, A.; Matziari, M.; Beau, F.; Cuniasse, P.; Yiotakis, A.; Dive, V. Development of potent and selective phosphinic peptide inhibitors of angiotensin-converting enzyme 2. *J. Med. Chem.* **2008**, *51*, 2216−2226.

(67) Guy, J. L.; Jackson, R. M.; Acharya, K. R.; Sturrock, E. D.; Hooper, N. M.; Turner, A. J. Angiotensin-converting enzyme-2 (ACE2): comparative modeling of the active site, specificity requirements, and chloride dependence. *Biochemistry* **2003**, *42*, 13185−13192.

(68) Pedersen, K. B.; Sriramula, S.; Chhabra, K. H.; Xia, H.; Lazartigues, E. Species-specific inhibitor sensitivity of angiotensin-converting enzyme 2 (ACE2) and its implication for ACE2 activity assays. *Am. J. Physiol.: Regul., Integr. Comp. Physiol.* **2011**, *301*, R1293−R1299.

(69) Huang, L.; Sexton, D. J.; Skogerson, K.; Devlin, M.; Smith, R.; Sanyal, I.; Parry, T.; Kent, R.; Enright, J.; Wu, Q.-l.; et al. Novel peptide inhibitors of angiotensin-converting enzyme 2. *J. Biol. Chem.* **2003**, *278*, 15532−15540.

(70) Deaton, D. N.; Gao, E. N.; Graham, K. P.; Gross, J. W.; Miller, A. B.; Strelow, J. M. Thiol-based angiotensin-converting enzyme 2 inhibitors: P1 modifications for the exploration of the S1 subsite. *Bioorg. Med. Chem. Lett.* **2008**, *18*, 732−737.

(71) Huentelman, M. J.; Zubcevic, J.; Hernandez Prada, J. A.; Xiao, X.; Dimitrov, D. S.; Raizada, M. K.; Ostrov, D. A. Structure-based discovery of a novel angiotensin-converting enzyme 2 inhibitor. *Hypertension* **2004**, *44*, 903−906.

(72) Byrnes, J. J.; Gross, S.; Ellard, C.; Connolly, K.; Donahue, S.; Picarella, D. Effects of the ACE2 inhibitor GL1001 on acute dextran sodium sulfate-induced colitis in mice. *Inflammation Res.* **2009**, *58*, 819−827.

(73) Padhi, A. K.; Rath, S. L.; Tripathi, T. Accelerating COVID-19 research using molecular dynamics simulation. *J. Phys. Chem. B* **2021**, *125*, 9078−9091.

(74) Pham, T.-H.; Qiu, Y.; Zeng, J.; Xie, L.; Zhang, P. A deep learning framework for high-throughput mechanism-driven phenotype compound screening and its application to COVID-19 drug repurposing. *Nat. Mach. Intell.* **2021**, *3*, 247−257.

(75) Cáceres, T. B.; Thakur, A.; Price, O. M.; Ippolito, N.; Li, J.; Qu, J.; Acevedo, O.; Hevel, J. M. Phe71 in type III trypanosomal protein arginine methyltransferase 7 (TbPRMT7) restricts the enzyme to monomethylation. *Biochemistry* **2018**, *57*, 1349−1359.

(76) Thakur, A.; Somai, S.; Yue, K.; Ippolito, N.; Pagan, D.; Xiong, J.; Ellis, H. R.; Acevedo, O. Substrate-Dependent Mobile Loop Conformational Changes in Alkanesulfonate Monooxygenase from Accelerated Molecular Dynamics. *Biochemistry* **2020**, *59*, 3582−3593.

(77) Torres, J. E.; Baldiris, R.; Vivas-Reyes, R. Design of Angiotensin-converting Enzyme 2 (ACE2) Inhibitors by Virtual Lead Optimization and Screening. *J. Chin. Chem. Soc.* **2012**, *59*, 1394−1400.

(78) Nami, B.; Ghanaeian, A.; Ghanaeian, K.; Nami, N. The effect of ACE2 inhibitor MLN-4760 on the interaction of SARS-CoV-2 spike protein with human ACE2: a molecular dynamics study. *ChemRxiv* **2020**, DOI: 10.26434/chemrxiv.12159945.v1.

(79) Cao, L.; Goreshnik, I.; Coventry, B.; Case, J. B.; Miller, L.; Kozodoy, L.; Chen, R. E.; Carter, L.; Walls, A. C.; Park, Y.-J.; et al. De novo design of picomolar SARS-CoV-2 miniprotein inhibitors. *Science* **2020**, *370*, 426−431.

(80) Mehranfar, A.; Izadyar, M. Theoretical Design of Functionalized Gold Nanoparticles as Antiviral Agents against Severe Acute Respiratory Syndrome Coronavirus 2 (SARS-CoV-2). *J. Phys. Chem. Lett.* **2020**, *11*, 10284−10289.

(81) Raghavan, P. Metadichol, a novel nano lipid formulation that inhibits SARS-COV-2 and a multitude of pathologicalviruses in vitro. *Res Square* **2020**, 1−31.

(82) Williams-Noonan, B. J.; Todorova, N.; Kulkarni, K.; Aguilar, M.-I.; Yarovsky, I. An Active Site Inhibitor Induces Conformational Penalties for ACE2 Recognition by the Spike Protein of SARS-CoV-2. The. *J. Phys. Chem. B* **2021**, 2533−2550.

(83) Liu, H.; Lupala, C.; Li, X.; Lei, J.; Chen, H.; Qi, J.; Su, X., Computational simulations reveal the binding dynamics between human ACE2 and the receptor binding domain of SARS-CoV-2 spike protein. *BioRxiv* **2020**.

(84) Casalino, L.; Gaieb, Z.; Goldsmith, J. A.; Hjorth, C. K.; Dommer, A. C.; Harbison, A. M.; Fogarty, C. A.; Barros, E. P.; Taylor, B. C.; McLellan, J. S.; et al. Beyond Shielding: The Roles of Glycans in the SARS-CoV-2 Spike Protein. *ACS Central Science* **2020**, 1722−1734.

(85) Arantes, P. R.; Saha, A.; Palermo, G., In; ACS Publications, 2020.

(86) Sztain, T.; Ahn, S.-H.; Bogetti, A. T.; Casalino, L.; Goldsmith, J. A.; Seitz, E.; McCool, R. S.; Kearns, F. L.; Acosta-Reyes, F.; Maji, S.; et al. A glycan gate controls opening of the SARS-CoV-2 spike protein. *Nat. Chem.* **2021**, 963−968.

(87) Humphrey, W.; Dalke, A.; Schulten, K. VMD - Visual Molecular Dynamics. *J. Mol. Graphics* **1996**, *14*, 33−38.

(88) Sastry, G. M.; Adzhigirey, M.; Day, T.; Annabhimoju, R.; Sherman, W. Protein and ligand preparation: parameters, protocols, and influence on virtual screening enrichments. *J. Comput.-Aided Mol. Des.* **2013**, *27*, 221−234.

(89) Case, D. A.; Ben-Shalom, I. Y.; Brozell, S. R.; Cerutti, D. S.; Cheatham, T. E., III; Cruzeiro, V. W. D.; Darden, T. A.; Duke, R. E.; Ghoreishi, D.; Giambasu, G.; Giese, T.; Gilson, M. K.; Gohlke, H.; Goetz, A. W.; Greene, D.; Harris, R.; Homeyer, N.; Huang, Y.; Izadi, S.; Kovalenko, A.; Krasny, R.; Kurtzman, T.; Lee, T. S.; LeGrand, S.; Li, P.; Lin, C.; Liu, J.; Luchko, T.; Luo, R.; Man, V.; Mermelstein, D. J.; Merz, K. M.; Miao, Y.; Monard, G.; Nguyen, C.; Nguyen, A. O.; Pan, F.; Qi, R.; Roe, D. R.; Roitberg, A.; Sagui, C.; Schott-Verdugo, S.; Shen, J.; Simmerling, C. L.; Swails, J.; Walker, R. C.; Wang, J.; Wei, H.; Wilson, L.; Wolf, R. M.; Wu, X.; Xiao, L.; Xiong, Y.; York, D. M.; Kollman, P. A. *AMBER*; University of California: San Francisco, 2019.

(90) Wang, J.; Wolf, R. M.; Caldwell, J. W.; Kollman, P. A.; Case, D. A. Development and testing of a general amber force field. *J. Comput. Chem.* **2004**, *25*, 1157−1174.

(91) Anandakrishnan, R.; Aguilar, B.; Onufriev, A. V. H++3.0: automating pK prediction and the preparation of biomolecular structures for atomistic molecular modeling and simulations. *Nucleic Acids Res.* **2012**, *40*, W537−W541.

(92) Maier, J. A.; Martinez, C.; Kasavajhala, K.; Wickstrom, L.; Hauser, K. E.; Simmerling, C. ff14SB: Improving the Accuracy of Protein Side Chain and Backbone Parameters from ff99SB. *J. Chem. Theory. Comput.* **2015**, *11*, 3696−3713.

(93) Kirschner, K. N.; Yongye, A. B.; Tschampel, S. M.; Gonzalez-Outeirino, J.; Daniels, C. R.; Foley, B. L.; Woods, R. J. GLYCAM06: a generalizable biomolecular force field. Carbohydrates. *J. Comput. Chem.* **2008**, *29*, 622−55.

(94) Jorgensen, W. L.; Madura, J. D.; Swenson, C. J. Optimized intermolecular potential functions for liquid hydrocarbons. *J. Am. Chem. Soc.* **1984**, *106*, 6638−6646.

(95) Li, P. F.; Roberts, B. P.; Chakravorty, D. K.; Merz, K. M. Rational design of particle mesh ewald compatible Lennard-Jones parameters for +2 metal cations in explicit solvent. *J. Chem. Theory Comput.* **2013**, *9*, 2733−2748.

(96) Li, P.; Song, L. F.; Merz, K. M., Jr. Systematic parameterization of monovalent Ions employing the nonbonded model. *J. Chem. Theory Comput.* **2015**, *11*, 1645−57.

(97) Ryckaert, J. P.; Ciccotti, G.; Berendsen, H. J. C. Numerical-Integration of Cartesian Equations of Motion of a System with Constraints - Molecular-Dynamics of N-Alkanes. *J. Comput. Phys.* **1977**, *23*, 327−341.

(98) Becke, A. D. Becke's three parameter hybrid method using the LYP correlation functional. *J. Chem. Phys* **1993**, *98*, 5648−5652.

(99) Francl, M. M.; Pietro, W. J.; Hehre, W. J.; Binkley, J. S.; Gordon, M. S.; DeFrees, D. J.; Pople, J. A. Self-consistent molecular orbital methods. XXIII. A polarization-type basis set for second-row elements. *J. Chem. Phys.* **1982**, *77*, 3654−3665.

(100) Frisch, M. J.; Trucks, G.; Schlegel, H.; Scuseria, G.; Robb, M.; Cheeseman, J.; Scalmani, G.; Barone, V.; Petersson, G.; Nakatsuji, H.et al.*Gaussian 09*; Gaussian, Inc.: Wallingford, CT, 2016.

(101) Pettersen, E. F.; Goddard, T. D.; Huang, C. C.; Couch, G. S.; Greenblatt, D. M.; Meng, E. C.; Ferrin, T. E. UCSF Chimera—a visualization system for exploratory research and analysis. *J. Comput. Chem.* **2004**, *25*, 1605−1612.

(102) DeLano, W. L. *Pymol: An open-source molecular graphics tool. CCP4 Newsletter on proteincrystallography*, 2002.

(103) *Schrödinger Release. 1: Maestro*; Schrödinger, LLC: New York, NY, 2017.

(104) Mol, A. R.; Castro, M. S.; Fontes, W. NetWheels: A web application to create high quality peptide helical wheel and net projections. *BioRxiv* **2018**, No. 416347.

https://doi.org/10.1021/acs.jcim.1c01283
J. Chem. Inf. Model. XXXX, XXX, XXX−XXX